ARTICLE

Display of lead-binding proteins on *Escherichia coli* surface for lead bioremediation

Xiaoqiang Jia[1,2,3] | Ying Li[1] | Tao Xu[1] | Kang Wu[4]

[1]Department of Biochemical Engineering, School of Chemical Engineering and Technology, Tianjin University, Tianjin, China

[2]Frontier Science Center for Synthetic Biology, Key Laboratory of Systems Bioengineering (MOE), School of Chemical Engineering and Technology, Tianjin University, Tianjin, China

[3]Collaborative Innovation Center of Chemical Science and Engineering (Tianjin), Tianjin, China

[4]Department of Chemical Engineering, University of New Hampshire, Durham, New Hampshire

Correspondence
Xiaoqiang Jia, Department of Biochemical Engineering, School of Chemical Engineering and Technology, Tianjin University, Tianjin 300072, China.
Email: xqjia@tju.edu.cn

Kang Wu, Department of Chemical Engineering, University of New Hampshire, Durham, NH 03824.
Email: Kang.Wu@unh.edu

Abstract

Cell surface display of heavy metal-binding proteins has been used to enhance the adsorption capacity of heavy metals and the engineered microbial cells can be potentially used for the bioremediation of heavy metals. In this study, the proteins PbrR, PbrR691, and PbrD from the *Cupriavidus metallidurans* strain CH34 were displayed on the extracellular membrane of *Escherichia coli* BL21 cells, with the N-domain of ice-nucleation protein as the anchor protein to achieve specific adsorption of lead ions (Pb^{2+}) and bioremediation of lead in the soil. The localization of fusion proteins was confirmed by western blot analysis. We investigated the effects of fusion pattern, expression level, heavy metal concentration, and the presence of other heavy metal ions on the adsorption of Pb^{2+} by these engineered bacteria, and the optimal linker peptide (flexible linker) and inducer concentration (0.5 mM) were obtained. The engineered bacteria showed specific selectivity and strong adsorption capacity for Pb^{2+}. The maximum Pb^{2+} adsorption capacity of strains displaying the three proteins (PbrR, PbrR691, and PbrD) were 942.1-, 754.3-, and 864.8-μmol/g cell dry weight, respectively, which was the highest reported to date. The engineered *E. coli* bacteria were also applied to Pb^{2+}-contaminated soil and the detoxification effects were observed via the seed germination test and the growth of *Nicotiana benthamiana* in comparison with the control BL21, which provides the proof-of-concept for in situ remediations of Pb^{2+}-contaminated water or soil.

KEYWORDS
cell-surface display, lead, *Nicotiana benthamiana*, PbrD, PbrR, PbrR691

1 | INTRODUCTION

With the advancement of civilized society and the rapid development of the world economy, the impact of human activity on the environment is becoming increasingly severe. Heavy metal pollution has emerged as a global concern due to industrialization and the popularity of motor vehicles (Sankhla, Kumari, Nandan, Kumar, & Agrawal, 2016; S. Singh et al., 2017). However, unlike other organic pollutants, heavy metals in the environment cannot be easily degraded; they can persist for a long time and remain in the soil for decades. This not only destroys the balance of the ecological environment (Gong, Huang, & Liu, 2018), but also eventually threatens the existence of living organisms by penetrating into food chains (Fatima & Ahmed, 2018; Siddiqui, Tauseef, & Bansal, 2018). Among these heavy metals, lead (Pb) is a cumulative toxicant that affects multiple body systems and particularly harmful to young children, causing damage to their nervous, hematopoietic, and immune systems, as well as affect their intelligence and growth (Murata, Iwata, Dakeishi, & Karita, 2009). It was identified by the World Health Organization as the most severe environmental poison threat to children (X. Wu et al., 2017).

To date, various techniques, such as chemical precipitation, chemical oxidation and reduction, ion exchange, filtration, electrochemical treatment, and reverse osmosis, have been used for heavy metal ions adsorption (Arief, Trilestari, Sunarso, Indraswati, & Ismadji, 2008). However, these remediation procedures are expensive, disruptive, highly detrimental to environmental sustainability, and inefficient in low-concentration environments. Compared to these physicochemical methods, bioremediation has become prominent in the field of heavy metal removal due to its high removal efficiency, low price, and small impact on the environment. Bioremediation generally includes phytoremediation and microbial adsorption (Wilson & Jones, 1993). Phytoremediation refers to the action of "super-accumulating plants" to absorb heavy metal ions through their root systems and transform pollutants into compounds that the plants can use for enrichment. However, its applications are limited because plants have slow growth rates, low biomass, and long repair cycles (Xiao, Li, Feng, & Shi, 2019). Some microorganisms are able to immobilize heavy metal ions inside their cells through bioenrichment. For example, Rani, Souche, and Goel (2009) found that the *Pseudomonas putida* strain 62BN significantly reduced the cadmium (Cd) content in the soil and that Cd was accumulated in cells as visualized by transmission electron microscopy. Other studies have shown that the *Cupriavidus metallidurans* strain CH34 contains a unique Pb^{2+} regulatory mechanism that can transport Pb^{2+} into cells and store them within the periplasm in the form of phosphate (Hobman, Julian, & Brown, 2012). However, bacterial cells have limited enrichment capacities and a lack of specificity for metal adsorption. Besides, the toxicity caused by excessive intracellular accumulation of heavy metals considerably affects the growth of bacterial cells.

Recently, the application of cell surface display has become the focus of many studies as an innovative method to enhance the adsorption selectivity and the capacity of specific metal ions extracellularly by anchoring specific heavy metal-binding proteins or peptides on the bacterial surface (Hettiarachchi & Pierzynski, 2004; Kuroda & Ueda, 2006; Shroff & Vaidya, 2012). According to the study by Bae, Wu, Kostal, Mulchandani, and Chen (2003), the ability of microbial cells to adsorb mercury (Hg) was enhanced by displaying the mercury binding protein MerR on the surface of *Escherichia coli* cells. In addition, engineered *Moraxella* sp. with synthetic phytochelatins (EC20) displayed on the surface had an increased adsorption capacity to mercury by more than 10-fold (Bae, Mulchandani, & Chen, 2002). Tao et al. (2016) displayed the metal-binding protein T68CadR on the surface of *Saccharomyces cerevisiae* and the engineered cells showed specific adsorption toward Cd^{2+}. The protein PbrR was displayed on the surface of *E. coli* to improve the binding ability of cells to Pb^{2+} (C. Hui et al., 2018; Wei, Liu, Sun, & Wang, 2014). Cell surface display of heavy metal-binding proteins has been proved as an effective strategy to improve the adsorption capacity of the microbes, but so far, only a few heavy metal-binding proteins were tested. For example, the study on Pb^{2+} bioremediation using this strategy is limited to the transcription factor PbrR. Further research is needed to optimize the surface display system and expand the pool of lead-binding proteins to further enhance the adsorption capacity.

The *pbr* operon from the *C. metallidurans* strain CH34 strain confers this strain lead resistance and it encodes proteins that specifically bind to Pb^{2+}, which can be potentially used for lead biosensing and bioremediation (Hobman et al., 2012). The expression of all of the genes in this operon is regulated by the transcription factor PbrR. In the presence of Pb^{2+}, the PbrR protein specifically binds to Pb^{2+} and initiates the expression of genes in the operon (P. Chen et al., 2005; Hobman et al., 2012). Proteins PbrTABC in *pbr* are related to the transport, energy supply, and phosphorylation of Pb^{2+}, which depend on proper function of the cell membrane, whereas PbrD acts as a lead-storing protein, which is related to the accumulation of Pb^{2+} in the cytoplasm and can effectively prevent the free transfer of Pb^{2+} within the cell (Borremans, Hobman, Provoost, Brown, & van der Lelie, 2001). Some studies have been devoted to developing whole-cell biosensors based on the transcription regulator PbrR and its cognate promoter for Pb^{2+} detection (Bereza-Malcolm, Aracic, & Franks, 2016; Jia, Ma, Bu, Zhao, & Wu, 2020; Wei et al., 2014). These biosensors demonstrated excellent sensitivity and specificity toward Pb^{2+} and may be used as a concentration monitoring tool for Pb^{2+}-contaminated water bodies. Due to its excellent binding characteristics to Pb^{2+}, PbrR was the first protein that was studied for Pb^{2+} bioremediation by cell-surface display. It was displayed on the surface of *E. coli*, and the adsorption capacity of cells to Pb^{2+} was increased by around 5–8 times compared to the control cells that did not display PbrR (C. Hui et al., 2018; Wei et al., 2014). The potential application of PbrD for lead bioremediation was explored by Keshav, Franklyn, and Kondiah (2019). PbrD was cross-linked to calcium alginate nanoparticles (CANPs), and the adsorption rate of the rPbrD–CANPs complex for Pb^{2+} reached 2.64 times than that of bare CANP at a concentration of 100 mg/L Pb, suggesting that pbrD has a great potential for Pb^{2+} adsorption. In addition, a PbrR homolog, PbrR691, was identified from the *C. metallidurans* CH34 genome. It demonstrates specificity toward Pb^{2+} 1,000 times higher than toward other metal ions (P. R. Chen et al., 2007). It has been used in the development of protein-based lead biosensors since it is more soluble than PbrR (P. Chen et al., 2005), but has not been studied for Pb^{2+} bioremediation. Overall, previous studies have indicated that PbrR, PbrR691, and PbrD all have strong and specific binding properties toward Pb^{2+}. Moreover, they are all soluble proteins that can be easily displayed on the cell surface, whereas the other proteins in this operon are transmembrane proteins which are not a proper candidate for cell surface display. But so far only PbrR has been examined for Pb^{2+} adsorption via cell surface display. In the few studies of displaying PbrR on the bacterial cell surface, the Pb^{2+} adsorption capacity is not very high, suggesting room to improve using engineering methods. In this study, these three proteins were each displayed on the surface of *E. coli* and the promoter, linker, protein expression level, and Pb^{2+} concentration were optimized to achieve higher Pb^{2+} adsorption capacity.

Cell surface display of a protein is achieved by fusing it with a protein naturally present on the cell surface and this natural protein is called an anchor protein. The selection of the anchor proteins is critical for the cell surface display efficiency. Currently, commonly used anchor proteins include the artificial chimeric protein Lpp-OmpA from *E. coli* (C. Hui et al., 2018) and the ice-nucleation protein

(INP) from *P. syringae* (Bloois, Winter, Kolmar, & Fraaije, 2011). INP is an outstanding outer membrane anchoring protein similar to eukaryotic glycosylphosphatidylinositol, which is composed of the N- and C-terminal domains and the intermediate repeat domain (M. L. Wu, Tsai, & Chen, 2006). At present, INP of various lengths have been successfully used to display proteins on the surface of *E. coli* cells (Daehwan & Seockmo, 2018; Fan, Liu, Yu, Yang, & Chen, 2011). Fan and colleagues used three different anchoring motifs, full-length INP (INP), truncated INP with N- and C-domains plus the first two and last three internal repeating subunits (INP-NC), and N-domain (INPN) to display the carbonic anhydrase (CA) on the surface of *E. coli* cells (Fan et al., 2011). Analysis by whole-cell ELISA showed that the fusion protein using the INPN as the anchor had a higher expression level, and the activity of CA fused with INPN was 1.7 times of that using the full-length INP and 2.9 times of that using the INP-NC. The INPN demonstrated better properties as an anchor in both promoting the expression level of the fusion protein and maintaining the functionality of the target protein, and thus it was selected as the anchor motif in this study. In addition, selecting a suitable linker between the two protein domains in the fusion protein can preclude protein misfolding, low protein yield, or impaired bioactivity (X. Chen, Zaro, & Shen, 2013; Huang, Li, Zhang, & Xing, 2016). These strategies can be used to engineer bacteria by displaying functional Pb^{2+} binding protein on the bacterial cell surface to adsorb or remove Pb^{2+}, but reports related to this are very limited.

In this study, three proteins from *C. metallidurans* CH34, PbrR, PbrR691, and PbrD, were each displayed on the cell surface of *E. coli* BL21 to investigate their adsorption of Pb^{2+}. The INPN from the *P. syringae* gene *inaK* (Accession No. NC AF013159) was used as the anchor protein to display these proteins. They were fused separately by end-to-end fusion (no linker [NL]) or by adding one of three commonly used linkers to examine the effect of linker on the functionality of the displayed proteins. The display of the protein on the cell surface was confirmed by cell fractionation, sodium dodecyl sulfate-polyacrylamide gel electrophoresis (SDS-PAGE), and western blot analysis. The engineered bacteria were endowed with an enhanced ability to adsorb Pb^{2+} and also markedly reduced the biological toxicity of heavy metals in contaminated soil.

2 | MATERIALS AND METHODS

2.1 | Bacterial strains, plasmids, and cultivation conditions

The *E. coli* strain BL21 (DE3) was used as a host strain for displaying a fusion protein and a wild-type bacterium as the control group. The plasmids p2-pbr harboring the PbrR-, PbrR691-, and PbrD-encoding genes and p2-inak harboring the partial gene sequences of INP, which are stored in our laboratory, were used as templates for the amplification of related genes. Unless stated otherwise, all *E. coli* bacteria were grown in Luria–Bertani (LB) broth containing 5 g/L yeast extract, 10 g/L sodium chloride, and 10 g/L peptone with an adjusted pH of 7.2–7.4. The plasmid pET-28a(+) containing the T7 promoter was used as the vector for cloning and protein expression. The initial culture temperature for all bacteria was 37°C. Once the bacteria had grown to the logarithmic growth phase (optical density [OD_{600}] = 0.6–0.8), the temperature was shifted to 22°C to induce the expression of proteins.

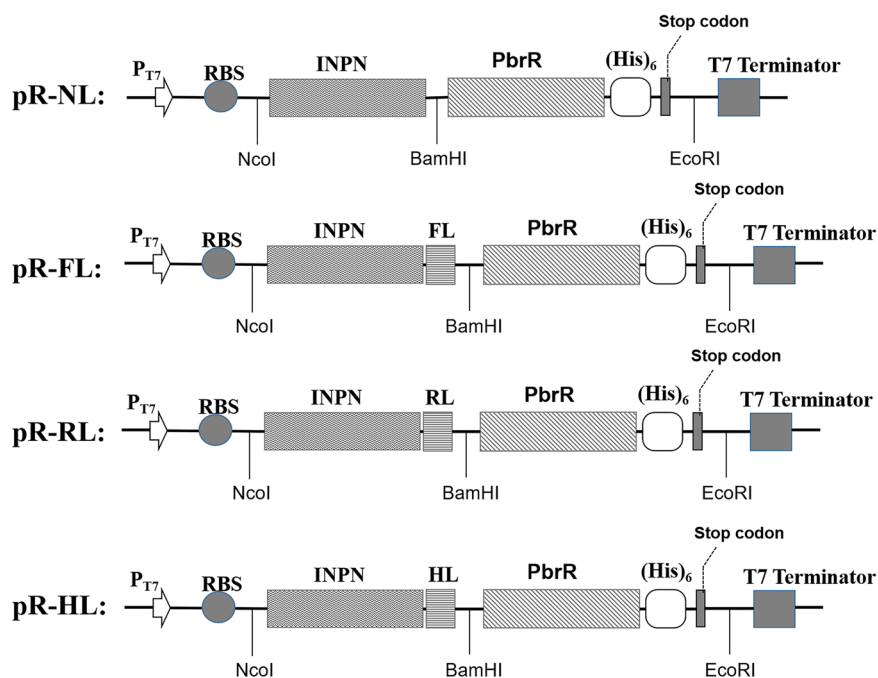## 2.2 | Plasmid construction

The PbrR, PbrR691, and PbrD surface display vectors were each paired with INPN coded by the *P. syringae* gene *inaK* (Accession no. NC AF013159) as an anchor. The engineered plasmid vectors were constructed first by polymerase chain reaction (PCR) amplification of the carrier proteins (INPNs) and passenger proteins (PbrR, PbrR691, and PbrD). Primers used for amplification are shown in Table 1. Primers P1 and P2 were used to amplify the INPN-encoding fragment (537 bp) using p2-inak preserved in our laboratory as a template. Three different linker peptides were used: flexible linker (FL) peptide composed of four glycines and one serine (GGGGS), rigid linker (RL) peptide rich in proline (PAPAP), or the rigid helical linker (HL) peptide AEAAAKEAAAKA. The coding sequences with different linker peptides of INPN were amplified via PCR using the forward primer P1 and reverse primers P3, P4, or P5, resulting in three types of INPN-linker fragments, namely INPN–FL (552 bp), INPN–RL (552 bp), and INPN–HL (537 bp). To construct fusion proteins, the stop codon of the four INP fragments were removed (Jung, Park, Park, Lebeault, & Pan, 1998). Both amplified fragments were digested with *Nco*I and *Bam*HI restriction enzymes. Primers P6 and P7 were used to amplify a 435-bp fragment of a PbrR-encoding fragment, with p2-pbr harboring PbrR-, PbrR691-, or PbrD-encoding genes as a template. For ease of detection, the downstream primer P7 carried a (His)$_6$-Tag. The amplified PbrR coding sequence was digested with *Bam*HI and *Eco*RI. The digested INPs and PbrR coding sequences were fused by T4 DNA ligase. The fusion fragments were digested with *Nco*I and *Eco*RI, and then inserted into the plasmid pET-28a(+) digested by the same restriction enzymes, resulting in plasmids pR–NL, pR–FL, pR–RL, and pR–HL (Figure 1). The PbrR691-encoding gene (396 bp) was amplified using primers P8 and P9, and the PbrD-coding sequence was amplified using primers P10 and P11. As previously described, a series of recombinant plasmids (i.e., pR691–NL, pR691–FL, pR691–RL, pR691–HL, pD–NL, pD–FL, pD–RL, and pD–HL) were constructed separately. All restriction enzymes were purchased from TransGen Biotech Co., Ltd. Plasmid extraction kits, PCR product purification kits, and agarose gel recovery kits were purchased from BioMed Biotech Co., Ltd.

2.3 | Cell growth and protein expression

First, a single colony of each bacterium containing the target plasmid was picked and precultured overnight in 3–5-ml LB medium containing kanamycin sulfate to a final concentration of 50 μg/ml at 37°C

TABLE 1 Primers used for the construction of recombinant plasmids

Primer	Sequence (5′-3′)	Restriction site
P1	CATGCCATGGGCATGACCCTGGATAAAGCACTGG	NcoI
P2	CGGGATCCGGTCTGCAGATTCTGCGGTGTGG	BamHI
P3	CGGGATCCGGAACCACCACCACCGGTCTGCAGATTCTGCGGTGTGG	BamHI
P4	CGGGATCCTGGAGCTGGAGCTGGGGTCTGCAGATTCTGCGGTGTGG	BamHI
P5	CGGGATCCAGCCTTAGCAGCAGCCTCCTTAGCAGCAGCCTCAGCGGTCTGCAGATTCTGCGGTGTGG	BamHI
P6	CGGGATCCATGAACATTCAGATTGGTGAACTGGC	BamHI
P7	CCGGAATTCTTAATGATGATGGTGATGATGATCGCTCGGATGTGCGGTGGTGCCAC	EcoRI
P8	CGGGATCCATGATGCGTATTGGTGAACTGGG	BamHI
P9	CCGGAATTCTTAATGATGATGGTGATGATGTGCAGGTTCTGCCAGGCTATTCAG	EcoRI
P10	CGGGATCCATGATGCCGGTTTATCTGGCCGATC	BamHI
P11	CCGGAATTCTTAATGATGATGGTGATGATGACGACATGCAT	EcoRI
	AGGCACCATCATTAC	

"——" represents restriction enzymes. "〰〰"represents different linkers. In P3, it implies FL (Gly-Gly-Gly-Gly-Ser); in P4, it implies RL (Pro-Ala-Pro-Ala-Pro); in P5, it implies HL (Ala-Glu-Ala-Ala-Ala-Lys-Glu-Ala-Ala-Ala-Lys-Ala); "═══"represents (His)₆-Tag.

Abbreviations: FL, flexible linker; HL, helical linker; RL, rigid linker.

FIGURE 1 Construction map of recombinant plasmids. A (His)$_6$-Tag sequence was added before the stop codon of the fusion proteins to facilitate detection. FL, flexible linker; HL, helical linker; INPN, N-domain of ice-nucleation protein; NL, no linker; PT7, T7 promoter; RBS, ribosome-binding site; RL, rigid linker

in a constant temperature shaker to revive the bacteria. Wild-type control was included. These mixtures were transferred to a 250-ml Erlenmeyer flask containing 100-ml LB medium without antibiotics for subculture at an inoculation rate of 2%. Once the cell concentration reached the logarithmic growth phase with an OD$_{600}$ of 0.6–0.8, the inducer isopropyl-β-D-thiogalactopyranoside (IPTG) was added to each flask to a final concentration of 0.2–2 mM. In heavy metal adsorption tests, Pb(NO$_3$)$_2$ was added to a final concentration of 50–2,000 μM. The culture of all bacteria was centrifuged at 8,000 rpm for 10 min to separate cell pellets and culture supernatant for subsequent experimental analysis. All experiments were performed in triplicates.

2.4 | Cell fractionation and western blot analysis

To study the specific location of the target protein on the cell surface of *E. coli*, cells were fractionated according to the methods reported previously (Li, Gyun Kang, & Joon Cha, 2004) to obtain the extracellular membrane, inner membrane, and cytoplasm. After 24 hr of induction at low temperature, all cell precipitates were collected and washed with phosphate-buffered saline (PBS) buffer three times and resuspended in 20-ml PBS buffer. The cells were disrupted with an ultrasonic disruptor for 10 min (intermittent 5-s pulse and rest periods) and centrifuged at 8,000 rpm for 10 min to remove cell debris. The supernatants were transferred to ultracentrifuge tubes (Beckman ultracentrifuge) for 1 hr at 39,000 rpm. The resulting supernatant contained the cytoplasmic component, whereas the pellet contained the membrane component. Pellets were resuspended in PBS buffer containing 0.01 mM MgCl$_2$ and 2% (vol/vol) Triton X-100. The suspension was incubated at room temperature for 30 min to

dissolve the cell membrane components and centrifuged at 39,000 rpm for 1 hr. The final precipitate contained components of the outer cell membrane, whereas the supernatant contained components of the inner cell membrane. Each fraction obtained by fractionation of the same volume was further analyzed.

To detect the expression of fusion proteins with a (His)$_6$-Tag and its location on the cell membrane, 20 μl of whole-cell lysate or different fractions obtained by cell fractionation were mixed with 5 μl SDS-PAGE loading buffer and placed in a boiling water bath for 10 min for complete protein denaturation. Proteins were separated by SDS-PAGE and transferred to a polyvinylidene fluoride membrane using a Bio-Rad standard wet transfer device. Membranes were blocked in TBST buffer containing 5% (wt/vol) skim milk for 2 hr. Rabbit anti-His immunoglobulin G (IgG) at a dilution of 1:1,000 was used as the primary antibody and rabbit anti-IgG with conjugated horseradish peroxidase at a dilution of 1:200 as the secondary antibody. After washing with TBST buffer several times, proteins were detected using western fluorescence detection reagent and developed on an X-ray film.

2.5 | Metal adsorption by engineered bacterial

To study the effects of the fusion method and linker type on the adsorption of Pb^{2+} by fusion proteins, engineered *E. coli* containing the plasmids pR–R691–D-NL, pR–R691–D-FL, pR–R691–D-RL, or pR–R691–D-HL were cultured to the logarithmic growth phase with an OD$_{600}$ of 0.6–0.8. Then, the inducer IPTG was added to a final concentration of 0.5 mM, and Pb(NO$_3$)$_2$ was added to a final concentration of 200 μM. After culturing at 22°C at 220 rpm for 12 hr, the cells were collected, washed with ddH$_2$O three times, dried in an

oven at 60°C for 24 hr, and weighed. The samples were digested in microwaves, and the Pb^{2+} content was determined by atomic absorption spectroscopy. After obtaining the optimal fusion method, the corresponding bacterium was selected for subsequent experiments.

This study also investigated the effects of different inducer concentrations (0, 0.2, 0.5, 1.0, 1.5, or 2.0 mM) and Pb^{2+} concentrations (50, 100, 300, 500, 1,000, or 2,000 μM) on the adsorption of Pb^{2+} by the engineered bacteria as well as the adsorption specificity of three target proteins under the coexistence of mixed metal ions (Pb^{2+}, Cd^{2+}, Hg^{2+}, and arsenic ion [As^{3+}]).

2.6 │ Germination of *Nicotiana benthamiana* seeds

To investigate the actual detoxification effect of engineered strains displaying PbrR, PbrR691, and PbrD, seed germination tests of *N. benthamiana* were designed. A presterilized filter paper was laid flat on the bottom of a sterile petri dish, and 100 tobacco seeds were distributed on the filter paper. The PbrR-, PbrR691-, or PbrD-displaying *E. coli* and wild-type strain BL21 were induced to culture in LB medium supplemented with 0.5-mM IPTG for 24 hr, and the cells were collected by centrifugation (8,000 rpm for 10 min). After washing three times with distilled water, the cell pellets were resuspended in ddH₂O to prepare a bacterial solution with OD_{600} of 3, and Pb^{2+} were added to the solution to a final concentration of 2,000 μM. A volume of 10 ml of each cell suspension was added to a Petri dish containing tobacco seeds. All Petri dishes were incubated at 28°C for 3 days under irradiation with white light. When seed coat rupture was visible, the seeds were considered to have germinated. The germination rate of seeds was calculated and analyzed. The germination state of seeds was observed under the optical Nikon E200 microscope and the seed germination rates were statistically analyzed by the F test.

2.7 │ Soil detoxification and plant growth

Cell suspensions of the PbrR-, PbrR691-, or PbrD-displaying bacteria and the wild-type strain BL21 as described in Section 2.6 were added with Pb(NO₃)₂ to a final concentration of 500 μM. Sterile plant growth nutrient soil (including standard peat soil, perlite, and vermiculite) was sterilized by autoclaving and mixed with the cell suspension at a ratio of 1:1 (wt/vol) to achieve the final concentration of Pb(NO₃)₂ in the soil of 500 μmol/kg. The treated soil was distributed in pots (100 mg per pot). *N. benthamiana* seedlings (30 days old) were selected and transplanted into the soil with two plants per pot. Plants were placed in a sunny greenhouse and watered every 2 days. After 50 days of incubation, the plants were weighed, and the chlorophyll content of the plant leaves was determined.

3 │ RESULTS AND DISCUSSION

3.1 │ Construction of INPN surface expression vectors

Through a series of molecular biological pathways such as restriction endonuclease digestion, fragment linkage, and plasmid transformation, plasmids carrying the gene *pbrR*, *pbrR691*, or *pbrD* were successfully constructed and expressed in BL21, with INPN as the anchoring motif. To ensure the correct folding of the target protein in the fusion state, four fusion patterns were designed to fuse the lead-binding protein with INPN: (a), NL; (b), a FL peptide composed of four glycines and one serine (GGGGS); (c), a RL peptide rich in proline (PAPAP); and (d), a rigid HL peptide AEAAAKEAAAKA. This results in plasmids pR–NL, pR–FL, pR–RL, pR–HL, pR691–NL, pR691–FL, pR691–RL, pR691–HL, pD–NL, pD–FL, pD–RL, and pD–HL, with R standing for PbrR, R691 for PbrR691, D for PbrD, NL for no linker, FL for the flexible linker, RL for the rigid linker, and HL for the rigid helical linker (Figure 1). The translation stop codon of INPN was removed, a (His)₆-Tag was added before the stop codon of PbrR, PbrR691, or PbrD for blot detection (see Section 2). To confirm the expressions of fusion proteins and their localization on cell surface, the whole-cell lysate of partially recombinant engineered bacteria and their different components obtained by cell fractionation were analyzed by western blot analysis. The molecular weight of PbrR, PbrR691, and PbrD is calculated to be 16.4, 15.2, and 26.7 kDa, respectively. With the addition of INPN (19 kD), linker (G₄S), and (His)₆-Tag, the molecular weight of the fusion protein is expected to be 36.6 (INPN–FL–PbrR), 35.5 (INPN–FL–PbrR691), and 46.9 kDa (INPN–FL–PbrD). Figure 2a shows that the target bands were seen at
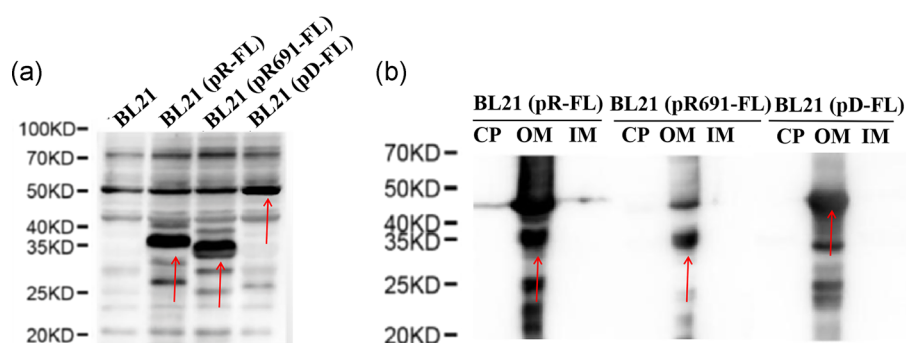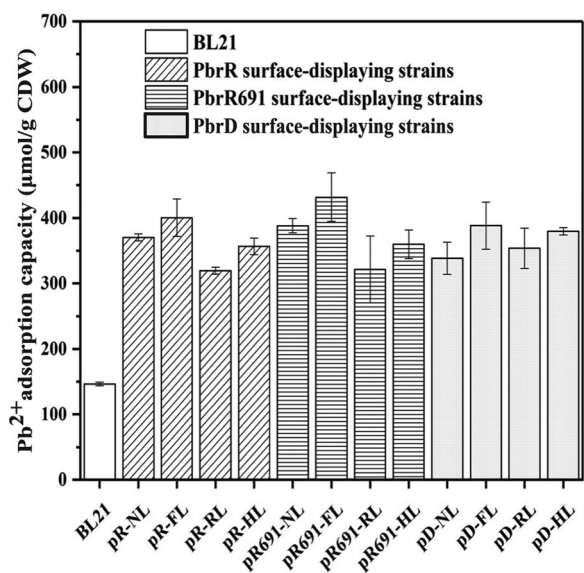

FIGURE 2 Western blot analysis of (a) whole-cell lysate and (b) cell fractionation. CP, cytoplasmic component; IM, inner cell membrane component; OM, outer cell membrane component [Color figure can be viewed at wileyonlinelibrary.com]

the corresponding molecular weight position, indicating the successful expression of the target proteins in the engineered bacteria. Cell fractionation demonstrated that target bands only appeared in the outer membrane fraction, confirming the location of the fusion proteins on the outer membrane.

3.2 | Comparison of the Pb^{2+} adsorption capacity of all engineered bacteria

Although all three proteins PbrR, PbrR691, and PbrD have demonstrated excellent Pb^{2+} binding properties in previous studies, they have not been compared and evaluated for lead bioremediation using cell surface display. To display them on the cell surface, the choice of the linker to make the fusion protein may affect the structure and function of the lead-binding protein. Therefore, to compare the Pb^{2+} adsorption capacity of PbrR, PbrR691, and PbrD displayed on *E. coli* surface and evaluate the effect of linker on the protein function, we first measured the Pb^{2+} adsorption per cell dry weight (CDW) of the strains displaying each of the three proteins fused with the anchor with NL, the FL, the RL, or the rigid HL with 0.5 mM of IPTG and 0.2 mM of Pb^{2+}. As shown in Figure 3, the Pb^{2+} adsorption capacity of all of the engineered bacteria displaying each of the three proteins was more than twice the control regardless of linker used, ranging from 319.7- to 431.7-μmol/g CDW, all of which were higher than the

adsorption capacity of Pb^{2+} in other studies (C. Y. Hui, Guo, Yang, Zhang, & Huang, 2018; C. Hui et al., 2018). The majority of Pb^{2+} adsorbed by the cells are due to the displayed proteins, and their performance is similar. On the basis of the highest adsorption capacity for each protein, the performance of PbrR691 (431.7-μmol/g CDW) is slightly better than that of PbrR (404.4-μmol/g CDW), followed by PbrD (388.4-μmol/g CDW). However, statistical analysis did not show a significant difference with $p > .05$. All three proteins are excellent candidates to make surface display strains for lead bioremediation. We also observed that the choice of linker has a notable effect on the adsorption capacity. For all three proteins, the use of the FL (G_4S) gave the highest Pb^{2+} adsorption capacity, with PbrR-FL achieving a Pb^{2+} adsorption capacity of 404.4-μmol/g CDW, PbrR691-FL at 431.7-μmol/g CDW, and PbrD–FL at 388.4-μmol/g CDW. This is not surprising because the flexibility and stability of the FL allow the target protein to fold properly and maximize the biological activity of the target protein in most cases (X. Chen et al., 2013; Hong et al., 2008). The effect of the other three linkers on the adsorption capacity was slightly different depending on the protein. For PbrR and PbrR691, the second-best linker choice was no linker (370.3- and 388.2-μmol/g CDW, respectively) while the linker with an α-helix (356.7- and 360.1-μmol/g CDW, respectively) and the RL (319.6- and 321.5-μmol/g CDW, respectively) gave the worst performance. It was opposite for PbrD, which prefers the linker with an α-helix (379.7-μmol/g CDW) and the RL (353.8-μmol/g CDW) over the one with no linker (338.5-μmol/g CDW). Statistical analysis showed that there were significant differences between different linkers for all three proteins with $p < .01$, which confirms that the choice of linker has a significant effect on the functionality of the fusion protein. In the follow-up study, only the engineered bacteria displaying the fusion proteins with the FL (G_4S) were selected for further characterization.

3.3 | Effect of the protein expression level on the Pb^{2+} adsorption capacity

IPTG is the inducer for gene expression from the T7 promoter. It regulates the gene expression at the transcription level and affects the accumulation level of biomass (Silaban, Gaffar, Simorangkir, Maksum, & Subroto, 2019). Excessively high concentrations of IPTG have potential toxicity (Rizkia et al., 2015). Therefore, we investigated the effect of different IPTG concentrations (0, 0.2, 0.5, 1.0, 1.5, or 2.0 mM) on cell growth and Pb^{2+} adsorption capacity of the engineered bacteria. IPTG was added after the cell concentration reached the logarithmic growth phase ($OD_{600} = 0.6–0.8$), and the OD_{600} of the culture was monitored until 12 hr after the IPTG induction. The effect of IPTG on cell growth is shown in Figure 4. The three engineered strains, each displaying PbrR, PbrR691, and PbrD with an FL, all reached a stable growth within 12 hr after the addition of IPTG regardless of the IPTG concentration. The OD_{600} was around 1.0 for the strain displaying PbrR, 1.2 for the one displaying PbrR691, and 1.3 for the one displaying PbrD. Without IPTG, the cells actively
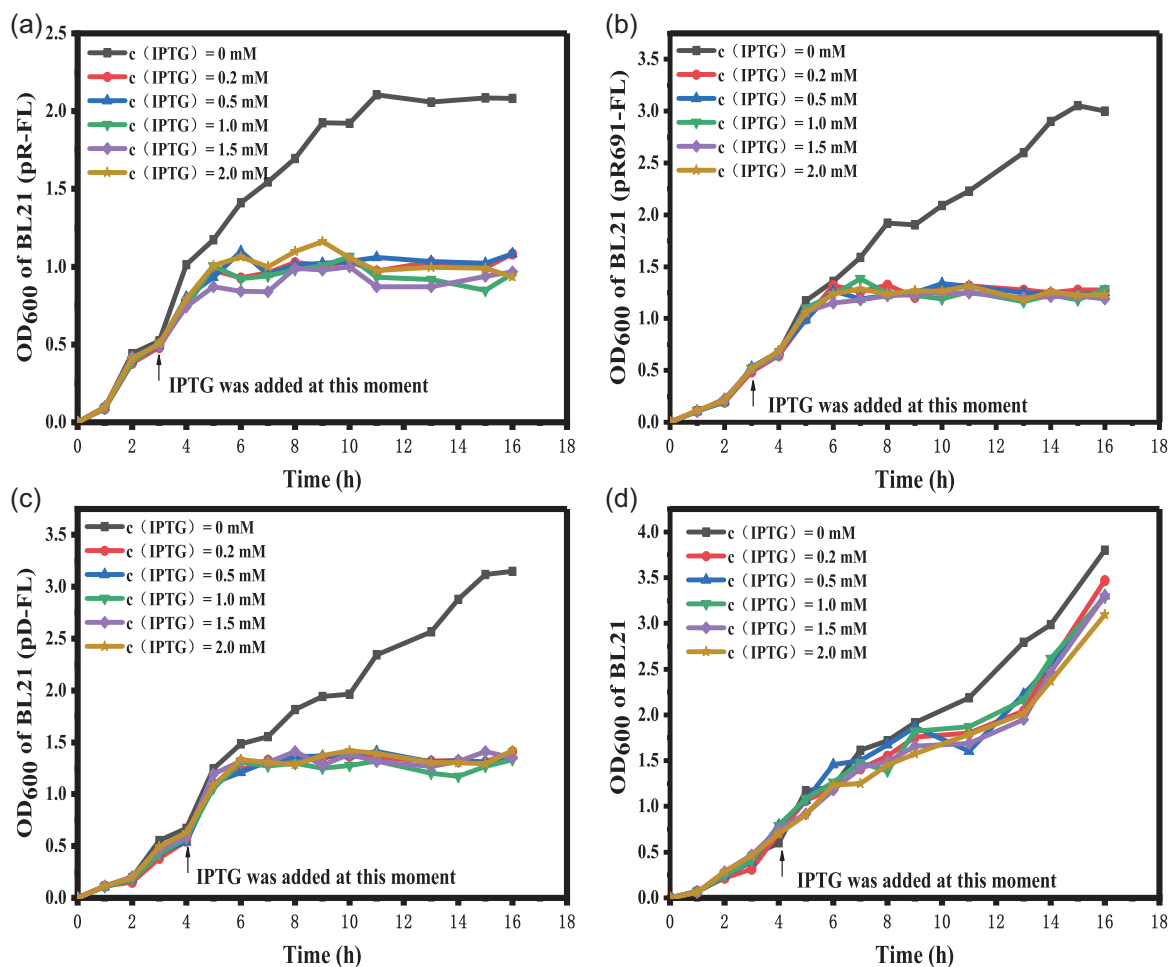

FIGURE 3 The adsorption capacity of all engineered bacteria on Pb^{2+}. Blank columns represent the wild-type strain BL21, columns filled with oblique lines represent PbrR-displaying bacteria, columns filled with horizontal lines represent PbrR691-displaying bacteria, and columns filled with small black dots represent PbrD-displaying bacteria. Among these, pR/R691/D–NL represents an end-to-end fusion between INP and target proteins (no linker), whereas pR/R691/D–FL represents fusion by a flexible linker (FL), pR/R691/D–RL represents fusion by a rigid linker (RL), and pR/R691/D–HL represents fusion by a helical linker (HL). CDW, cell dry weight

FIGURE 4 Effect of IPTG concentration on the growth status of all tested strains. (a) BL21 (pR–FL), (b) BL21 (pR691–FL), (c) BL21 (pD–FL), and (d) wild-type strain BL21 (DE3). FL, flexible linker; IPTG, isopropyl-β-D-thiogalactopyranoside; OD, optical density [Color figure can be viewed at wileyonlinelibrary.com]

grew for a longer period and their growth was much better, with a stable OD around 2.0 for the strain displaying PbrR, 3.0 for the one displaying PbrR691, and 3.1 for the one displaying PbrD. Clearly, among the three lead-binding proteins, the overexpression of PbrR exerted a greater burden on the cell growth, while the other two gave a much higher eventual OD. This may be associated with the difference in the surface properties of these proteins. In one study using PbrR as the sensing component of a lead biosensor, it was mentioned that PbrR691 was preferred because it was more soluble than PbrR (P. Chen et al., 2005). Overexpression of a protein with relatively lower solubility could affect both the cellular and cell surface conditions more severely. A thorough characterization of the solubility of these proteins is necessary to verify this hypothesis. In contrast, the effect of IPTG on the control BL21 was minimal. With and without IPTG, BL21 constantly grew within the period of characterization and did not reach a plateau. The OD_{600} slightly decreased from 3.8 to 3.0 as the concentration of IPTG increased from 0 to 2.0 mM. Compared to the control, it is clear that the expression of the fusion protein displayed on the cell surface affected the cell
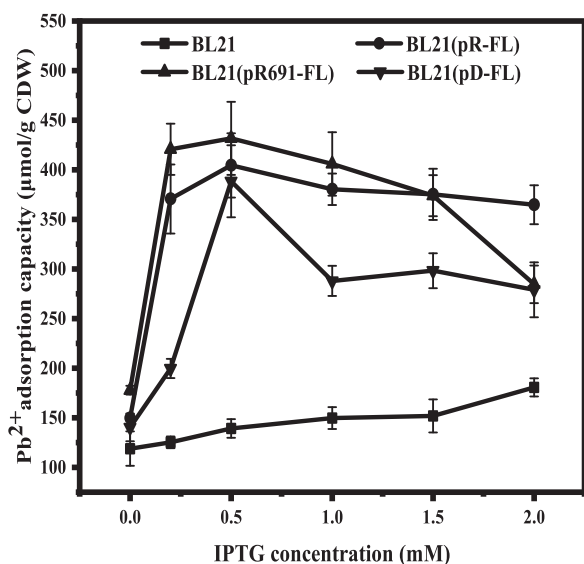
growth, which entered the stationary phase soon after the induction of the expression. This suggests the expression of the fusion proteins presents a significant burden to the cells.

Since the displayed lead-binding proteins are responsible for the adsorption of the majority of the Pb^{2+}, as shown in Figure 3, the Pb^{2+} adsorption capacity is expected to increase as the protein expression level increases. However, the overexpression of these fusion proteins in presence of the inducer IPTG triggered bacterial stasis, as discussed in the last paragraph, and the local cellular and cell surface environments are likely to change accordingly, which may undermine the function of the displayed lead-binding proteins. Moreover, the expression of the heterologous protein often reaches an upper limit due to the limited recourse in the cell. Therefore, an optimal inducer concentration is expected to give the maximum adsorption capacity. To investigate the effect of the protein expression level, the Pb^{2+} adsorption capacity of the three engineered strains each displaying PbrR, PbrR691, and PbrD, as well as the control BL21, were measured at different concentrations of IPTG (0, 0.2, 0.5, 1.0, 1.5, and 2.0 mM). No signs of protein inactivation or the formation of

inclusion bodies due to protein overexpression were observed in this study, so we assume that the lead-binding affinity of the displayed proteins stays about the same regardless of the expression level.

As shown in Figure 5, the Pb^{2+} adsorption capacity of all demonstrated a peak when the concentration of IPTG was 0.5 mM, while that of the control BL21 steadily and slowly increased from 118.9- to 180.7-μmol/g CDW when the concentration of IPTG went from 0 to 2.0 mM. The peak values of the three engineered strains were very close, about 3.1, 2.9, and 2.8 times of the control BL21 for PbrR691, PbrR, and PbrD respectively. But the difference is not significant with a P-value higher than 0.05. The strains displaying PbrR and PbrR691 showed a sharp increase at low concentrations of IPTG and their adsorption capacity at 0.2 mM of IPTG were close to their peak value at 0.5 mM of IPTG, while the curve for the one displaying PbrD concaved up when the concentration of IPTG is lower than 0.5 mM. When the concentration of IPTG was above 0.5 mM, the adsorption capacity of the strain displaying PbrR declined slowly, but the ones displaying PbrR691 and PbrD showed a greater decrease. It seemed from this graph that the effect of protein overexpression on the adsorption capacity of the PbrR-displaying strain was less than the other two, although it presented a higher burden to the growth of the cells displaying PbrR (Figure 4). We speculate that certain properties of PbrR, such as lower solubility, cause cells to grow slower to accommodate the overexpression and surface display of PbrR, but the lead-binding properties of PbrR is relatively stable in response to cellular change due to protein overexpression. In contrast, the lead-binding properties of PbrR691 and PbrD are more affected by the protein expression level. The stability of these proteins needs to be further investigated by characterizing the dissociation constant of these lead-binding proteins at different concentrations of the protein, which will be the next step of our future work. In this study, 0.5 mM of IPTG will be used in the subsequent experiments.

3.4 | Effects of heavy metal concentration and species on Pb^{2+} adsorption

To determine the effect of Pb^{2+} concentrations on the adsorption capacity of the engineered bacteria, the bacterial strains were incubated in LB medium containing different concentrations of Pb^{2+} (50–2,000 μM) for 12 hr. It is worth noting that the LB medium in this study contains 10 g/L of NaCl, which may cause the precipitation of Pb^{2+} at high concentrations. However, the solubility of $PbCl_2$ in water is 1/100 g water (35.96 mM) at 20°C, and it increases as the temperature goes up. According to the calculation formula of precipitation equilibrium constant $K_{sp} = [Pb^{2+}] [Cl^-]^2$, we determined the solubility of $PbCl_2$ in 10 g/L NaCl as 6.36 mM at 20°C. The solubility of $PbCl_2$ in 10 g/L NaCl at 22°C, the temperature used in this study, is expected to be slightly higher than the calculated value at 20°C. The maximum Pb^{2+} concentration used in this study is 2 mM which is below this value. So the precipitation of $PbCl_2$ is negligible.

The effect of Pb^{2+} concentration on adsorption capacity of the engineered bacteria was shown in Figure 6, the Pb^{2+} adsorption capacity of all bacteria first increased as the concentrations of Pb^{2+} increased until it reached a peak, and then it started to decrease as the Pb^{2+} concentration further increased. However, under high concentrations of Pb^{2+}, the adsorption capacity of Pb^{2+} by the engineered bacteria gradually diminished. One possible explanation is that the displayed proteins on the cell surface are saturated at high concentrations of Pb^{2+}. Another reason is that as the concentration of Pb^{2+} goes up, lead toxicity is not negligible and it will inhibit cell
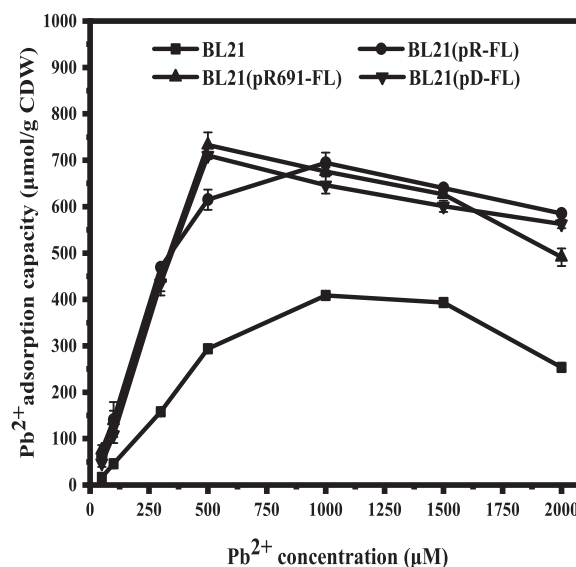

FIGURE 5 Effect of IPTG concentration on the adsorption of Pb^{2+} by the engineered bacteria. CDW, cell dry weight; FL, flexible linker; IPTG, isopropyl-β-D-thiogalactopyranoside


FIGURE 6 Effect of Pb^{2+} concentration on adsorption capacity of the engineered bacteria. CDW, cell dry weight; FL, flexible linker

growth and protein expression, thereby significantly reducing the adsorption capacity of the bacteria to Pb^{2+}. This could be addressed by increasing bacterial biomass used for lead bioremediation or using a multistage remediation process. Further increasing the copy number of the fusion proteins on the bacteria surface is also an option, but it is limited by the available cell surface area as well as the available energy/material of the cell, as it is shown that the overexpression of heterologous proteins often means a heavy metabolic burden to the cell and results in cell death or slow cell growth. The adsorption capacity of the bacteria displaying PbrR691 and PbrD showed a sharp increase to 732.8- and 710.1-μmol/g CDW as the concentration of Pb^{2+} rose from 0 to 500 μM and then gradually and linearly decreased as the concentration further went up. However, the bacterium displaying PbrR demonstrated a parabolic curve. After the initial sharp increase till the concentration of Pb^{2+} reached 300 μM, the adsorption capacity increased slower and reached a peak of 694.3-μmol/g CDW at 1,000 μM of Pb^{2+}. Then, it entered the decrease phase with a similar trend as the other two strains when the concentration of Pb^{2+} was between 1,000 and 1,500 μM, but then decreased much faster when the concentration was higher than 1,500 μM. This curve was very similar in trend to that of the control BL21, although the adsorption capacity of BL21 was much lower with the peak value at 408.8-μmol/g CDW. This is an interesting phenomenon as PbrR and PbrR691 are both transcription factors, while PbrD has a different function for lead storage. However, the lead adsorption performances of strains displaying PbrR691 and PbrD are similar, and PbrR showed a clearly different pattern. It seems that Pb^{2+} at high concentration has a greater effect on the function of PbrR compared to the other two proteins either because PbrR is more sensitive to Pb^{2+} at high concentrations or the function of PbrR is closely correlated to cellular function which is impacted at high concentrations of Pb^{2+}. It is noted that the overexpression of PbrR had a greater inhibitory effect on the cell growth as shown in Figure 3, suggesting a higher burden exerted to the cell by the presence of large amounts of PbrR. This could be synergistically amplified by the lead toxicity at high concentrations of Pb^{2+}. A thorough characterization of dissociation constants between the three proteins and Pb^{2+} under different concentrations of Pb^{2+} is necessary for the future to better understand the underlying reason. It will be also helpful to compare the binding affinity of soluble proteins and fusion proteins displayed on the cell surface to further study the effect of cell surface display on the function of the three proteins.

Compared to previous studies, the strains we constructed demonstrated higher adsorption capacity. C. Y. Hui et al. (2018) displayed PbrR on the surface of *E. coli* cells using Lpp-OmpA as the anchor protein and obtained the adsorption capacity up to 144-μmol/g CDW at 300 μM of Pb^{2+}. Our strains showed a capacity of 435.4–468.9-μmol/g CDW at the same concentration of Pb^{2+}. In another study, the *E. coli* displaying PbrR showed an accumulation of Pb^{2+} lower than 120 μmol/g Pb^{2+} (Wei et al., 2014), while our strains peaked around 700-μmol/g CDW. Clearly, through the optimization of the linker, promoter, protein expression level, and lead concentration, the Pb^{2+} adsorption capacity of the engineered bacteria

displaying lead-binding proteins has been significantly improved. All three proteins demonstrated excellent potential for lead bioremediation using the cell surface display strategy, though they showed a slight difference in the lead dose-response curve, which may provide insight in choosing the protein depending on the lead concentration in the system to be remediated.

The three lead-binding proteins used in this study, PbrR, PbrR691, and PbrD, are from the *pbr* operon which specifically senses and clears Pb^{2+}, and, thus, they demonstrate superb specificity when used in lead biosensing and bioremediation. Still, their specificity toward Pb^{2+} after being displayed on the cell surface needs to be assessed. In this study, we characterized the three engineered strains displaying each of the three proteins as well as the control BL21 for their adsorption capacity of mixed ions. A culture medium containing Pb^{2+}, Cd^{2+}, As^{3+}, and Hg^{2+} at a final concentration of 100, 500, or 1,000 μM was used to grow the bacteria in the same way as we measured the single ion Pb^{2+} adsorption capacity, followed by the inductively coupled plasma mass spectrometry analysis of ion concentrations. As shown in Figure 7, the Pb^{2+} adsorption capacity of the three engineered strains was dramatically higher than that of the control BL21. The strains displaying PbrR, PbrR691, and PbrD showed Pb^{2+} adsorption capacity 3.1–10.9, 2.7–8.2, and 3.0–9.3 times of the control, respectively. However, the Cd^{2+} and Hg^{2+} adsorption capacity of the three strains was similar to that of the control, about 0.94–1.70 times, which showed the displayed proteins specifically adsorbed Pb^{2+}. All of the strains showed negligible adsorption to As^{3+}, which is not surprising as key proteins such as the transcription factor in the arsenic sensing and resistance
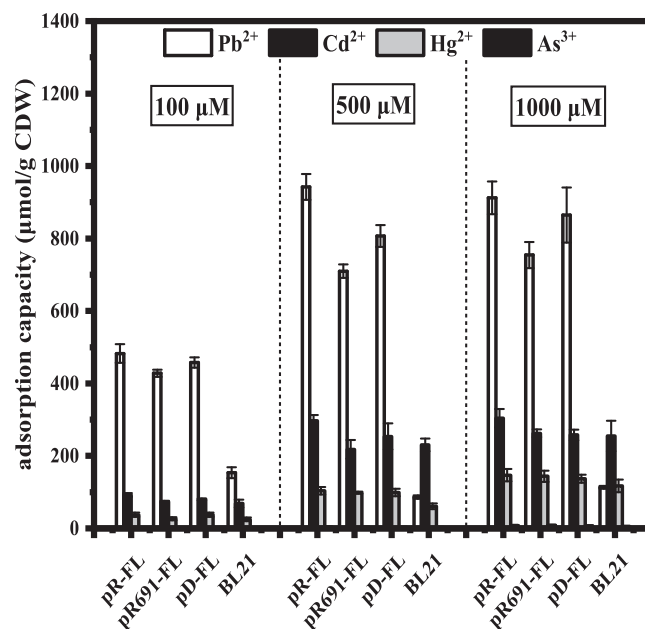
FIGURE 7 The adsorption capacity of all tested bacteria in mixed metal ion solutions containing lead, mercury, cadmium, and arsenic ions at different concentrations. Mixed metal ion concentrations were set to 100, 500, and 1,000 μM, respectively. CDW, cell dry weight; FL, flexible linker

operon do not belong to the same family of the transcription factor. The crosstalk between transcription factors from different families is minimal. Here, As^{3+} was included in this test as a negative control. The specificity of the three displayed proteins toward Pb^{2+} is comparable. At $100\,\mu M$ of all ions, the ratio of the adsorption capacity for Pb^{2+} over Cd^{2+} was 5.2 times for the strain displaying PbrR, and 5.8 times for the one displaying PbrR691, and 5.7 times for the one displaying PbrD. The ratio of the adsorption capacity for Pb^{2+} over Hg^{2+} was 13 times, 16.5 times, and 12.4 times for the three strains, respectively. At low concentrations of ions, the specificity of PbrR691 displayed on the cell surface is slightly better than the other two, but overall their performance is very similar.

As the concentration of the ions increased from 100 to $1,000\,\mu M$, the Pb^{2+} specificity of these strains evaluated by the Pb^{2+}/Cd^{2+} and Pb^{2+}/Hg^{2+} ratios slightly decreased. For the strain displaying PbrR, these two ratios decreased to 3.2 and 9.1 at $500\,\mu M$ of mixed ions and further decreased to 3.0 and 6.2 as the concentration went up to $1,000\,\mu M$. The ratios for the strain displaying PbrR691 dropped to 3.3 and 7.2 at $500\,\mu M$ of mixed ions, and further decreased to 2.9 and 5.2 as the concentration went up to $1,000\,\mu M$. Similarly, the strain displaying PbrD showed changed ratios of 3.2 and 8.2 at $500\,\mu M$ of mixed ions, and 3.4 and 6.3 at $1,000\,\mu M$. It can be seen that the other ions at high concentrations interfere with the binding of these proteins to Pb^{2+}, likely due to the stress caused by high concentrations of heavy metal ions, which affects the cellular and surface environments of cells and also the structure and function of these proteins, making them less selective in divalent ions.

Though quantitative biochemical data on the Pb^{2+} binding affinity and specificity are lacking, computational modeling has provided some insight into the extraordinary adsorption properties of these lead-binding proteins. Tolbatov, Re, Coletti, and Marrone (2019) investigated the binding of Pb^{2+} at pbrR by means of multiscale computational modeling and found that the three cysteine motifs in the pbrR structure play a leading role. By changing the protonation state of the Cys3 motif, PbrR can explore a wide range of lead affinity. Therefore, the compartmentalization of lead-binding motifs (somehow related to the homodimerization) is the main effector of the lead affinity of PbrR (Tolbatov et al., 2019). The study of Taghavi et al. (2008) also pointed out that the high selectivity of PbrR691 for Pb^{2+} is mainly attributed to the unique semidirectional geometry of the

lead coordination center, so that Pb^{2+} can be preferentially recognized by PbrR691 through chelation effects. The PbrD protein inactivation test shows that PbrD acts as a molecular chaperone of Pb^{2+} and can chelate with Pb^{2+} to reduce the level of free lead in the cytoplasm (Taghavi et al., 2008). However, there are few studies on the structural characteristics of PbrD relevant to its affinity for Pb^{2+}.

Related studies have shown that the MerR protein from the specific regulatory framework of Hg^{2+}, the CadR protein related to the specific binding of Cd^{2+}, and the PbrR and PbrR691 proteins (Borremans et al., 2001) all belong to the MerR family and have similar cysteine pocket structures arranged in tricoordinate (Brown, Stoyanov, Kidd, & Hobman, 2006; Hobman et al., 2012). Bivalent heavy metal ions prefer hemidirected geometry in 3- or 4-coordinate complexes (P. R. Chen et al., 2007). Therefore, MerR family proteins can bind to some divalent heavy metal ions. Studies by D. K. Singh, Lingaswamy, Koduru, Nagu, and Jogadhenu (2019) also proved that MerR family proteins are almost resistant to metals other than specific metals. The ArsR protein related to As^{3+} does not belong to this family (Jia, Bu, Zhao, & Wu, 2019), which explains why the engineered bacteria in this study were able to adsorb cadmium and mercury but had the little binding capacity to As^{3+}. The results of this study also indicated that PbrD appears to have similar adsorption effects as PbrR and PbrR691. A recent study by Keshav, Achilonu, Dirr, & Kondiah (2019) and Keshav, Franklyn et al. (2019) on the efficient remediation of Pb^{2+}-contaminated environment by PbrD demonstrated its ability to preferentially remediate Pb^{2+}, which was consistent with the conclusion of the present study.

3.5 | Germination of *N. benthamiana* seeds under lead stress

Heavy metal ions have toxic effects on seed germination and plant growth (Hettiarachchi & Pierzynski, 2004). The eventual effectiveness of the engineered bacteria in this study in lead bioremediation needs to be exemplified by their effect on plant seeding and growth. *N. benthamiana* seeds were used in this study to perform the germination test and subsequent biomass characterization. As shown in Table 2, the germination rate and average bud length of *N. benthamiana* seeds treated with the engineered *E. coli* cells and the

TABLE 2 Effects of lead ion on the germination rate of *Nicotiana benthamiana* seeds

Strain	Percentage of seed germination (%)	Average bud length (mm)	Seed micrograph
BL21	20.7 ± 1.5[a]	1.0 ± 0.2[b]	
BL21 (pR–FL)	51 ± 3.6[a]	8.5 ± 0.1[b]	
BL21 (pR691–FL)	55 ± 2.6[a]	7.9 ± 0.3[b]	
BL21 (pD–FL)	49 ± 3.5[a]	9.0 ± 0.3[b]	

Abbreviation: FL, flexible linker.
[a]Indicates that there is a significant difference in the percentage of seed germination between the wild-type bacteria BL21 and the PbrR/PbrR691/PbrD-displaying bacteria (F test, $p < .001$).
[b]Indicates that there is a significant difference in the average bud length between the wild-type bacteria BL21 and the PbrR/PbrR691/PbrD-displaying bacteria (F test, $p < .001$).

control BL21 in presence of 2,000 μM of Pb^{2+} were determined. Statistical analysis showed that there were significant differences between the PbrR-, PbrR691-, or PbrD-displaying bacteria and the control on the germination rate of *N. benthamiana* seeds. The germination rate of *N. benthamiana* seeds treated with the engineered bacteria was ~2.5 times higher than that of the control BL21. Moreover, the average bud length of *N. benthamiana* seeds treated with the engineered bacteria was over eight times higher than that of seeds treated with wild-type BL21, indicating that the engineered bacteria played an important role in alleviating the toxicity of Pb^{2+}. The effects of PbrR, PbrR691, and PbrD on seed germination rates were not significantly different, although the germination rate of seeds treated with PbrR691-displaying bacteria (55 ± 2.6%) was relatively higher than that of other two strains (51 ± 3.6% for the one displaying PbrR and 49 ± 3.5% for the one displaying PbrD).

These results showed that the PbrR-, PbrR691-, or PbrD-displaying bacteria can effectively detoxify Pb^{2+} and promote the germination of the seeds, which is consistent with previous studies using PbrR to protect seeds from the Pb^{2+} toxicity (Wei et al., 2014).

3.6 | Remediation of Pb^{2+} toxicity in soil

To determine whether the engineered bacteria can remediate the toxicity of Pb^{2+} in soil, a bioassay was set up to examine the fixation effect of Pb^{2+} in soil based on the growth status of *N. benthamiana*. *N. benthamiana* seedlings (30 days old) of uniform growth were transplanted into 500-μmol/kg nutrient soil treated by different strains. The growth of *N. benthamiana* plants in Pb^{2+}-contaminated soil for 20–50 days was shown in Figure 8. The *N. benthamiana*
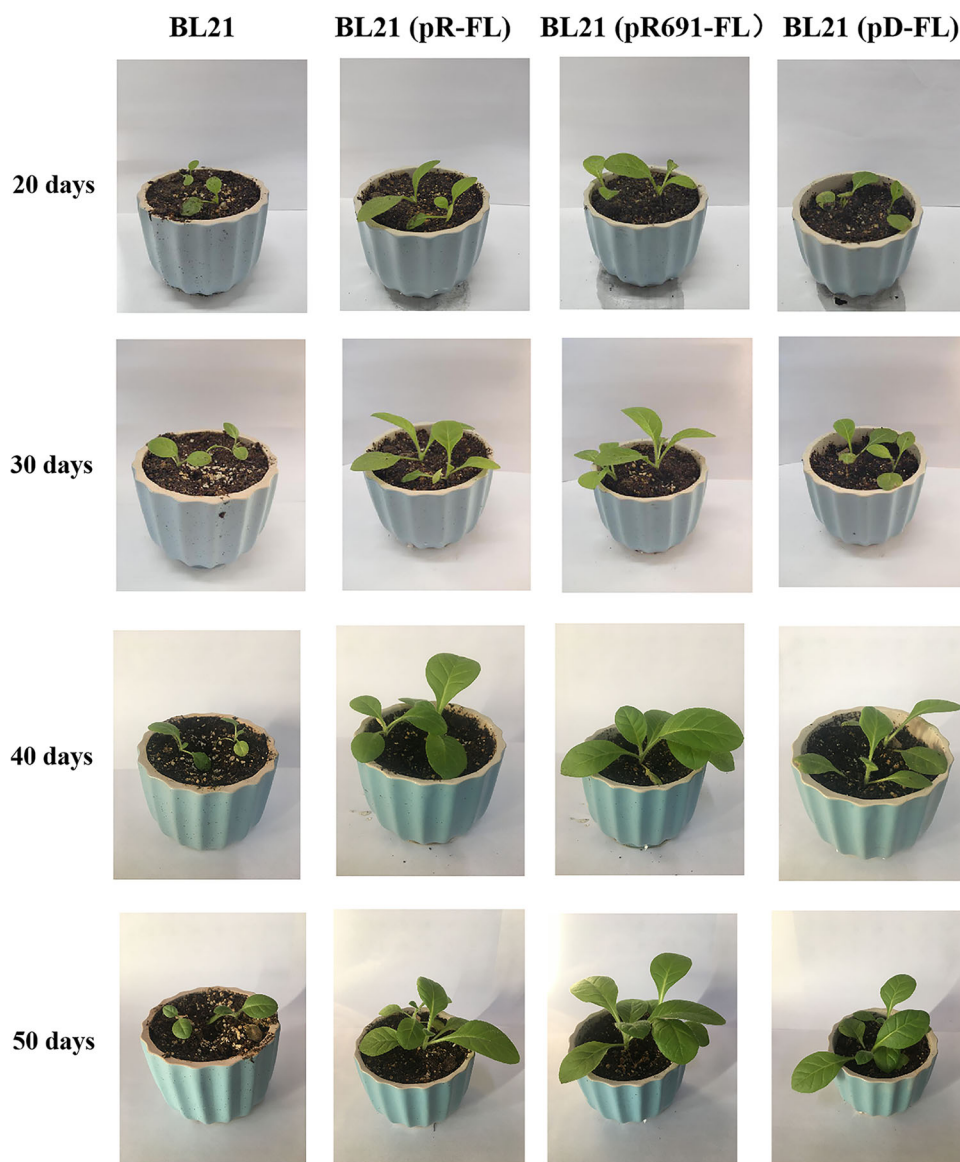
FIGURE 8 Growth status of *Nicotiana benthamiana* plants in lead-contaminated soil treated with different engineered bacteria. FL, flexible linker [Color figure can be viewed at wileyonlinelibrary.com]

TABLE 3 Effects of lead ion on *Nicotiana benthamiana* growth

Strain	Average biomass (g)	Average chlorophyll content (mg/g)
BL21	0.10 ± 0.02	1.07 ± 0.34
BL21 (pR–FL)	0.74 ± 0.21	1.12 ± 0.16
BL21 (pR691–FL)	1.34 ± 0.27	1.10 ± 0.19
BL21 (pD–FL)	0.73 ± 0.05	1.16 ± 0.20

Abbreviation: FL, flexible linker.

seedlings in the soil treated with the engineered bacteria BL21 (pR–FL), BL21 (pR691–FL), and BL21 (pD–FL) all grew well, but the seedlings planted in the pot treated with the wild-type strain BL21 showed poor growth, indicating the strong fixation ability of engineered bacteria to Pb^{2+} in soil within a limited observation period. To quantify these results, after 50 days of cultivation, the biomass and the chlorophyll content of *N. benthamiana* plants in each pot were measured. The data in Table 3 confirmed that the display of the lead-binding proteins on the cell surface enhanced the adsorption effect of the engineered bacteria to Pb^{2+} in soil (Valls, Atrian, de Lorenzo, & Fernández, 2000), thereby alleviating the toxicity of heavy metal ions in the soil, which was of great significance for the in situ bioremediation of heavy metal-contaminated soil.

4 | CONCLUSION

Both cell surface display and using PbrR for lead adsorption are not new. However, previous studies on lead-specific bioremediation using cell surface display mainly focused on the transcription factor PbrR (Wei et al., 2014; C. Y. Hui et al., 2018; C. Hui et al., 2018). Moreover, the adsorption capacity of the target strains to Pb^{2+} in the existing research was not very high. In addition to PbrR, the specific binding of PbrR691 and PbrD to Pb^{2+} has also been reported, suggesting them good candidates for lead bioremediation, However, they have not been examined for lead adsorption using cell surface display. In this study, PbrR, PbrR691, and PbrD from the lead resistance bacterium *C. metallidurans* CH34 were displayed on the surface of *E. coli* BL21 using INPN as the anchor protein to construct bacteria with specific adsorption properties for Pb^{2+}. Our results indicated the engineered strains displaying each protein all have excellent lead adsorption properties and identified key parameters that affect the adsorption capacity. First, it was found that the linker in the fusion protein had a noticeable effect on the efficiency of Pb^{2+} adsorption, and the one with the FL showed a slightly higher efficiency. Second, the expression level of the fusion proteins controlled by the concentration of the inducer IPTG directly affected the adsorption capacity of Pb^{2+}. The optimal concentration of IPTG for Pb^{2+} adsorption was found to be 0.5 mM, above which the adsorption capacity began to decrease, likely due to cellular stress from protein overexpression which may affect the function of the lead-binding proteins. Third, the concentration of Pb^{2+} in the environment was

also found to affect the Pb^{2+} adsorption capacity of cells. PbrR, PbrR691, and PbrD-displaying bacteria reached a maximum adsorption capacity of 694.3-, 732.8-, and 710.1-μmol/g CDW when the Pb^{2+} concentration was 1,000, 500, and 500 μM, respectively. Above the optimum concentration, the toxicity of the Pb^{2+} seems to impact cellular environments, and the function of these proteins. Moreover, the mixed metal adsorption test using Pb^{2+}, Cd^{2+}, Hg^{2+}, and As^{3+} showed that all three engineered bacteria showed relatively high specificity toward Pb^{2+}, those the selectivity of divalent ions becomes looser at high concentrations of ions. Previous studies have shown that both PbrR and PbrR691 bin to Pb^{2+} specifically (P. R. Chen et al., 2007; C. Y. Hui et al., 2018). Recent studies have also used PbrD to achieve Pb^{2+} adsorption in the environment (Keshav, Achilonu et al., 2019; Keshav, Franklyn et al., 2019). Our results further confirmed that these proteins as excellent candidates for specific bioremediation of Pb^{2+}, and also demonstrated they can all successfully displayed on the cell surface. Through the use of high-copy plasmids, a strong promoter, optimum fusion pattern and expression level, strong adsorption capacities, and high specificity for Pb^{2+} were achieved. Notably, a systematic comparison of Pb^{2+} adsorption characteristics of these three proteins showed a subtle difference between them. Displayed on the cell surface, PbrR seemed to have a stronger effect on the cell growth with a short exponential phase and lower OD than the other two. It was also more sensitive to the toxicity of Pb^{2+} or the cellular environmental change caused by Pb^{2+} at high concentrations. However, PbrR demonstrated better tolerance to cellular stress due to the overexpression of proteins and the strain displaying PbrR showed relatively steady adsorption capacity at very high concentrations of the inducer IPTG. These differences are likely attributed to the chemical and biochemical properties of these proteins, such as surface properties, solubility, binding affinity, and stability, which need to be further investigated.

To investigate the detoxification effect of the engineered bacteria on Pb^{2+} in the environment, *N. benthamiana* seed germination tests and *N. benthamiana* cultivation tests in Pb^{2+}-contaminated soil were conducted using previously reported methods (Valls et al., 2000; Wei et al., 2014). *N. benthamiana* seeds or plants treated with the engineered bacteria showed much better growth during the observation period compared to the control group, indicating that Pb^{2+} adsorption in the environment by the engineered bacteria was effective.

It is worth mentioning that this study has used engineered *E. coli* BL21(DE3) for plant seeds germination, seedling growth, and proved the detoxification effect although, *E. coli* is not a practical model for applications in the rhizosphere, and the feasible field application eventually requires *rhizobia* or other soil bacteria. However, *Rhizobacteria* generally coexists with plants and have a complicated genetic background, making them not suitable for basic verification studies. Unlike *Rhizobium*, *E. coli* has been widely used as the model organism for expressing and characterizing foreign genes in scientific research due to its clear genetic background, fast growth rate, and efficient genetic toolkits. In this study, *E. coli* with T7RNA polymerase coding ability and other excellent characteristics was used as a lab

model to quickly compare the three lead-binding proteins when displayed on the cell surface for lead bioremediation and test different designs, such as optimizing the fusion pattern and expression level. The development of indigenous microorganisms such as *Pseudomonas*, *Rhizobium*, and so forth with the optimized design to display these lead-binding proteins, need to be further developed in the future.

Overall, the results of this study are of great significance for reducing the toxicity of Pb^{2+} to cells, promoting the fixation of Pb^{2+} in the environment, and achieving in situ remediations of heavy metal-polluted environments.

CONFLICT OF INTERESTS

The authors declare that there are no conflict of interests.

ORCID

Xiaoqiang Jia http://orcid.org/0000-0002-1756-1926

REFERENCES

Arief, V. O., Trilestari, K., Sunarso, J., Indraswati, N., & Ismadji, S. (2008). Recent progress on biosorption of heavy metals from liquids using low cost biosorbents: Characterization, biosorption parameters and mechanism studies. *Clean—Soil Air Water*, 36(12), 937–962.

Bae, W., Mulchandani, A., & Chen, W. (2002). Cell surface display of synthetic phytochelatins using ice nucleation protein for enhanced heavy metal bioaccumulation. *Journal of Inorganic Biochemistry*, 88(2), 223–227.

Bae, W., Wu, C. H., Kostal, J., Mulchandani, A., & Chen, W. (2003). Enhanced mercury biosorption by bacterial cells with surface-displayed MerR. *Applied & Environmental Microbiology*, 69(6), 3176–3180.

Bereza-Malcolm, L., Aracic, S., & Franks, A. (2016). Development and application of a synthetically-derived lead biosensor construct for use in Gram-negative bacteria. *Sensors*, 16(12), 13.

Bloois, E. V., Winter, R. T., Kolmar, H., & Fraaije, M. W. (2011). Decorating microbes: Surface display of proteins on *Escherichia coli*. *Trends in Biotechnology*, 29(2), 79–86.

Borremans, B., Hobman, J. L., Provoost, A., Brown, N. L., & van der Lelie, D. (2001). Cloning and functional analysis of the pbr lead resistance determinant of *Ralstonia metallidurans* CH34. *Journal of Bacteriology*, 183(19), 5651–5658.

Brown, N. L., Stoyanov, J. V., Kidd, S. P., & Hobman, J. L. (2006). The MerR family of transcriptional regulators . *FEMS Microbiology Reviews*, 27(2-3), 145–163.

Chen, P., Greenberg, B., Taghavi, S., Romano, C., Lelie, D. V. D., & He, C. (2005). An exceptionally selective lead(II)-regulatory protein from *Ralstonia metallidurans*: Development of a fluorescent lead(II) probe. *Angewandte Chemie International Edition English*, 44(18), 2715–2719.

Chen, P. R., Wasinger, E. C., Zhao, J., van der Lelie, D., Chen, L. X., & He, C. (2007). Spectroscopic insights into lead(II) coordination by the selective lead(II)-binding protein PbrR691. *Journal of the American Chemical Society*, 129(41), 12350–12351.

Chen, X., Zaro, J. L., & Shen, W.-C. (2013). Fusion protein linkers: Property, design and functionality. *Advanced Drug Delivery Reviews*, 65(10), 1357–1369.

Daehwan, K., & Seockmo, K. (2018). Bacillus cellulase molecular cloning, expression, and surface display on the outer membrane of *Escherichia coli*. *Molecules*, 23(2), 503.

Fan, L. H., Liu, N., Yu, M.-R., Yang, S.-T., & Chen, H.-L. (2011). Cell surface display of carbonic anhydrase on *Escherichia coli* using ice nucleation protein for CO_2 sequestration. *Biotechnology and Bioengineering*, 108(12), 2853–2864.

Fatima, H., & Ahmed, A. (2018). Micro-remediation of chromium contaminated soils. *PeerJ*, 6, e6076.

Gong, X., Huang, D., Liu, Y., Peng, Z., Zeng, G., Xu, P., ... Wan, J. (2018). Remediation of contaminated soils by biotechnology with nanomaterials: Bio-behavior, applications, and perspectives. *Critical Reviews in Biotechnology*, 38(3), 455–468.

Hettiarachchi, G. M., & Pierzynski, G. M. (2004). Soil lead bioavailability and in situ remediation of lead-contaminated soils: A review. *Environmental Progress*, 23(1), 78–93.

Hobman, J. L., Julian, D. J., & Brown, N. L. (2012). Cysteine coordination of Pb(II) is involved in the PbrR-dependent activation of the lead-resistance promoter, PpbrA, from Cupriavidus metallidurans CH34. *BMC Microbiology*, 12(1), 109.

Hong, L. Z., Yao, X. Q., Xue, C., Wang, Y., Xiong, X. H., & Liu, Z. M. (2008). Increasing the homogeneity, stability and activity of human serum albumin and interferon-α2b fusion protein by linker engineering. *Protein Expression and Purification*, 61(1), 0–77.

Huang, Z., Li, G., Zhang, C., & Xing, X.-H. (2016). A study on the effects of linker flexibility on acid phosphatase PhoC-GFP fusion protein using a novel linker library. *Enzyme and Microbial Technology*, 83, 1–6.

Hui, C. Y., Guo, Y., Yang, X.-Q., Zhang, W., & Huang, X.-Q. (2018). Surface display of metal binding domain derived from PbrR on *Escherichia coli* specifically increases lead(II) adsorption. *Biotechnology Letters*, 47(5), 837–845.

Hui, C., Guo, Y., Zhang, W., Gao, C., Yang, X., Chen, Y., ... Huang, X. (2018). Surface display of PbrR on *Escherichia coli* and evaluation of the bioavailability of lead associated with engineered cells in mice. *Scientific Reports*, 8(1), 5685.

Jia, X., Bu, R., Zhao, T., & Wu, K. (2019). Sensitive and specific whole-cell biosensor for arsenic detection. *Applied and Environmental Microbiology*, 85(11), 10.

Jia, X., Ma, Y., Bu, R., Zhao, T., & Wu, K. (2020). Directed evolution of a transcription factor PbrR to improve lead selectivity and reduce zinc interference through dual selection. *AMB Express*, 10(1), 67.

Jung, H. C., Park, J. H., Park, S. H., Lebeault, J. M., & Pan, J. G. (1998). Expression of carboxymethylcellulase on the surface of *Escherichia coli* using *Pseudomonas syringae* ice nucleation protein. *Enzyme & Microbial Technology*, 22(5), 348–354.

Keshav, V., Achilonu, I., Dirr, H., & Kondiah, K. (2019). Recombinant expression and purification of a functional bacterial metallo-chaperone PbrD-fusion construct as a potential biosorbent for Pb (II). *Protein Expression and Purification*, 158, 27–35.

Keshav, V., Franklyn, P., & Kondiah, K. (2019). Recombinant fusion protein PbrD cross-linked to calcium alginate nanoparticles for Pb remediation. *ACS Omega*, 4(16), 16816–16825.

Kuroda, K., & Ueda, M. (2006). Effective display of metallothionein tandem repeats on the bioadsorption of cadmium ion. *Applied Microbiology & Biotechnology*, 70(4), 458–463.

Li, L., Gyun Kang, D., & Joon Cha, H. (2004). Functional display of foreign protein on surface of *Escherichia coli* using N-terminal domain of ice nucleation protein. *Biotechnology and Bioengineering*, 85(2), 214–221.

Murata, K., Iwata, T., Dakeishi, M., & Karita, K. (2009). Lead toxicity: Does the critical level of lead resulting in adverse effects differ between adults and children? *Journal of Occupational Health*, 51(1), 1–12.

Rani, A., Souche, Y. S., & Goel, R. (2009). Comparative assessment of in situ bioremediation potential of cadmium resistant acidophilic *Pseudomonas putida* 62BN and alkalophilic *Pseudomonas monteilli* 97AN strains on soybean. *International Biodeterioration & Biodegradation, 63*(1), 62–66.

Rizkia, P. R., Silaban, S., Hasan, K., Kamara, D. S., Subroto, T., Soemitro, S., & Maksum, I. P. (2015). Effect of Isopropyl-β-D-thiogalactopyranoside concentration on prethrombin-2 recombinan gene expression in *Escherichia coli* ER2566. *Procedia Chemistry, 17*, 118–124.

Sankhla, M. S., Kumari, M., Nandan, M., Kumar, R., & Agrawal, P. (2016). Heavy metals contamination in water and their hazardous effect on human health—A review. *International Journal of Current Microbiology and Applied Sciences, 5*(10), 759–766.

Shroff, K. A., & Vaidya, V. K. (2012). Effect of pre-treatments on the biosorption of chromium (VI) ions by the dead biomass of rhizopus arrhizus. *Journal of Chemical Technology & Biotechnology, 87*(2), 294–304.

Siddiqui, N. A., Tauseef, S. M., & Bansal, K. (2018). Human health effects emanating from airborne heavy metals due to natural and anthropogenic activities: A review, *Advances in health and environment safety* (pp. 279–296). Berlin, Germany: Springer.

Silaban, S., Gaffar, S., Simorangkir, M., Maksum, I. P., & Subroto, T. (2019). Effect of IPTG concentration on recombinant human prethrombin-2 expression in *Escherichia coli* BL21(DE3) ArcticExpress. *IOP Conference Series Earth and Environmental Science, 217*.

Singh, D. K., Lingaswamy, B., Koduru, T. N., Nagu, P. P., & Jogadhenu., P. S. S. (2019). A putative *merR* family transcription factor Slr0701 regulates mercury inducible expression of MerA in the cyanobacterium *Synechocystis* sp. PCC6803. *MicrobiologyOpen, 8*(9), e00838.

Singh, S., Tripathi, D. K., Singh, S., Sharma, S., Dubey, N. K., Chauhan, D. K., & Vaculík, M. (2017). Toxicity of aluminium on various levels of plant cells and organism: A review. *Environmental & Experimental Botany, 137*, 177–193.

Taghavi, S., Lesaulnier, C., Monchy, S., Wattiez, R., Mergeay, M., & van der Lelie, D. (2008). Lead(II) resistance in cupriavidus metallidurans CH34: Interplay between plasmid and chromosomally-located functions. *Antonie Van Leeuwenhoek, 96*(2), 171–182.

Tao, H. C., Li, P. S., Liu, Q. S., Su, J., Qiu, G. Y., & Li, Z. G. (2016). Surface-engineered *Saccharomyces cerevisiae* cells displaying redesigned CadR for enhancement of adsorption of cadmium (II). *Journal of Chemical Technology & Biotechnology, 91*(6), 1889–1895.

Tolbatov, I., Re, N., Coletti, C., & Marrone, A. (2019). Determinants of the lead(II) affinity in pbrR protein: A computational study. *Inorganic Chemistry, 59*(1), 790–800.

Valls, M., Atrian, S., de Lorenzo, V., & Fernández, L. A. (2000). Engineering a mouse metallothionein on the cell surface of Ralstonia eutropha CH34 for immobilization of heavy metals in soil. *Nature Biotechnology, 18*(6), 661–665.

Wei, W., Liu, X., Sun, P., Wang, X., Zhu, H., Hong, M., ... Zhao, J. (2014). Simple whole-cell biodetection and bioremediation of heavy metals based on an engineered lead-specific operon. *Environmental Science & Technology, 48*(6), 3363–3371.

Wilson, S. C., & Jones, K. C. (1993). Bioremediation of soil contaminated with polynuclear aromatic hydrocarbons (PAHs): A review. *Environmental Pollution, 81*(3), 229–249.

Wu, M. L., Tsai, C. Y., & Chen, T. H. (2006). Cell surface display of Chi92 on *Escherichia coli* using ice nucleation protein for improved catalytic and antifungal activity. *FEMS Microbiology Letters, 256*(1), 119–125.

Wu, X., Guo, Y., Hui, C., Chen, J., Gao, C., & Zeng, X. (2017). Growth characteristics of PbrR surface displayed *Escherichia coli* in vitro and in vivo. *China Tropical. Medicine, 17*(07), 650–654.

Xiao, Z., Li, G., Feng, J., & Shi, Y. (2019). Review and prospection of soil heavy metal remediation with combined earthworm-plant technology. *Environmental Chemistry, 38*(11), 2510–2518.